Journal of Materials Chemistry C

Accepted Manuscript

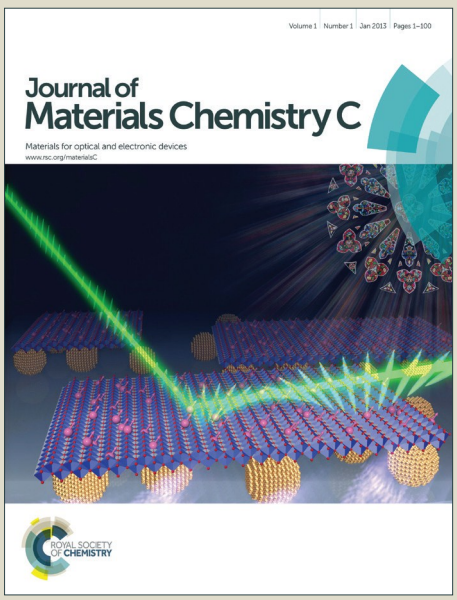

This is an *Accepted Manuscript*, which has been through the Royal Society of Chemistry peer review process and has been accepted for publication.

Accepted Manuscripts are published online shortly after acceptance, before technical editing, formatting and proof reading. Using this free service, authors can make their results available to the community, in citable form, before we publish the edited article. We will replace this *Accepted Manuscript* with the edited and formatted *Advance Article* as soon as it is available.

You can find more information about *Accepted Manuscripts* in the Information for Authors.

Please note that technical editing may introduce minor changes to the text and/or graphics, which may alter content. The journal's standard Terms & Conditions and the Ethical guidelines still apply. In no event shall the Royal Society of Chemistry be held responsible for any errors or omissions in this *Accepted Manuscript* or any consequences arising from the use of any information it contains.

ROYAL SOCIETY OF CHEMISTRY

www.rsc.org/materialsC

Journal Name

ARTICLE

DNA-Mediated Control of Au Shell Nanostructure and Controlled Intra-Nanogap for Highly Sensitive and Broad Plasmonic Response Range

Received 00th January 20xx,
Accepted 00th January 20xx

DOI: 10.1039/x0xx00000x

www.rsc.org/

Haemi Lee[a], Sang Hwan Nam[a], Yu Jin Jung[a], So-Jung Park[a], Jung-Mu Kim[b], Yung Doug Suh[a,c,*] and Dong-Kwon Lim[d,*]

We report the DNA-mediated simple synthetic methods to obtain anisotropic plasmonic nanostructures with a tailorable intra-nanogap distance ranging from 0.9 to 4.0 nm. Anisotropic half-shell structures with sub-1.0 nm intra-nanogaps showed a wavelength-independent surface-enhanced Raman scattering (SERS) intensity and a highly sensitive SERS response to NIR light. We found that the reaction conditions such as pH and NaCl concentration are responsible for the resulting shell structures and intra-nanogap distances. Three noticeable plasmonic nanostructures [i.e., half-shell with sub-1.0 nm nanogaps, closed-shell with wide nanogap (2.1 nm) and star-shaped with irregular nanogap (1.5–4.0 nm)] were synthesized, and solution-based and single particle-based Raman measurements showed the strong relationship between plasmonic structures and SERS intensity. An understanding of DNA-mediated control for nanogap-engineered plasmonic nanostructures and studies of SERS-activity relationships using single particle-correlated measurements can provide new insights into the design of new plasmonic nanostructures and SERS-based biosensing applications.

Introduction

DNA-mediated synthetic strategies enabled to build up precisely-controlled 2D or 3D plasmonic nanostructures which are challenging issue with a conventional chemistry.[1-4] DNA-mediated control over metallic nanoparticle shape also enabled to produce useful and unique nanostructures in a sequence specific manner.[5, 6] The recently developed gold nanoparticles with narrow intra-nanogaps (Au-NNPs) composed of core AuNP (20 nm) and Au shell (~10 nm thickness) showed uniform and strong SERS responses in solution with narrow SERS enhancement factor (EF) distributions ranging from 1.0×10^8 to 5.0×10^9.[7] The highly SERS-active nanoparticle because of localized Raman-dyes in the intra-nanogap (1.2 nm) is useful as a bright labelling material for SERS-based applications.[8-12] Developing new synthetic methods for Au-NNPs[9] and understanding for the Au shell growth mechanism including the role of DNA are of great interest.[13] Although the sequence dependent effects of DNA in generating the intra-nanogap already were unveiled in several research papers,[7, 14, 15] the reaction parameters have not been investigated yet.

In this report, we focused the effect of reaction parameters to provide clear understanding for the synthetic method of Au-NNPs and also to provide new plasmonic nanostructures that can overcome the current limitation of Au-NNP structures. In spite of the strong and uniform SERS response of Au-NNPs, there are two limitations for practical SERS-based applications. First, Au-NNPs cannot detect molecules present in the sample solution owing to their closed-shell structure. Second, the spherical geometry of Au-NNPs results in an intrinsically weak SERS response to near-infrared (NIR) excitation, which is required in order to minimize the fluorescence background for SERS-based cell imaging applications. Gold nanoshell structures have been investigated extensively,[16-18] and anisotropic nanostructures such as gold nanorods or gold nanostar have been studied in an effort to obtain a strong SERS response by use of the resonant localized surface plasmon resonance (LSPR) properties of these structures with an NIR excitation wavelength.[6, 19-22] However, the absence of a nanogap in these nanostructures offers limited SERS intensity especially in solution. In this regard, NIR-sensitive anisotropic nanoparticles with narrow and open intra-nanogaps dispersed in solution are essentially required for practical SERS-based sensing or imaging applications.[13, 23, 24]

In this work, we demonstrate the effect of reaction parameters such as specific pH and NaCl on the resulting Au shell structure and the plasmonic properties of obtained nanostructures. The shell structure was greatly varied by the reaction parameters. The intra-nanogap distance was tailorable on a nanoscale ranging from 0.9 nm to 4.0 nm. As a result, four unique nanostructures with different intra-nanogap distances and shell structures were obtained: half-

[a] Laboratory for Advanced Molecular Probing (LAMP), Korea Research Institute of Chemical Technology, Daejeon 305-600, South Korea
[b] Department of Electronic Engineering, Chonbuk National University, 567 Baeckje-daero, Jeonju 561-756, South Korea.
[c] School of Chemical Engineering, Sungkyunkwan University, Suwon 440-746, South Korea.
[d] KU-KIST Graduate School of Converging Science and Technology, Korea University, 145 Anam-ro, Soeongbuk-gu, Seoul 135-467, South Korea.
† Electronic Supplementary Information (ESI) available: Fig. S1-S8 as described in the text. See DOI: 10.1039/x0xx00000x

Journal of Materials Chemistry C Accepted Manuscript

Please do not adjust margins

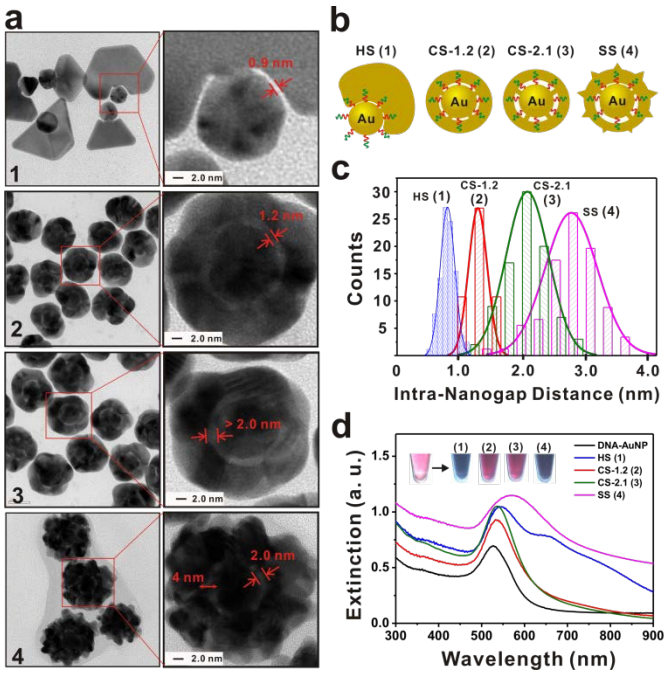

Figure 1. Four unique nanostructures and characterizations. (a) High-resolution transmission electron microscope (HR-TEM) images and magnified images of selected area (red-colored box). (b) Brief sketch of resulting nanostructures. (c) Distributions of intra-nanogap distance (based on the TEM image analysis, N = 50). (d) Extinction spectra of DNA-AuNP (black), HS (1) (blue line), CS-1.2 (2) (red line), CS-2.1 (3) (green line), and SS (4) (magenta line). Inset: solution color of nanostructures.

shell structures with open, sub-1.0-nm intra-nanogaps [~0.9 nm, HS (1)], closed-shell structures with intra-nanogaps of ~1.2 nm [CS-1.2 (2)], closed-shell structures with wider intra-nanogap structures [~2.1 nm, (CS-2.1 (3)], and star-shaped structures with irregular intra-nanogaps (1.5–4.0 nm) [SS (4)] (Figures 1 and S1). Solution-based measurements, single particle-based correlated Raman measurements, and finite element method (FEM) lab-based theoretical studies were performed to investigate the optical properties of those four nanostructures and their relationships to SERS activity. HS (1) exhibited a very strong SERS response with an NIR excitation wavelength of 785 nm, as well as with shorter wavelengths (532, 660 nm). In contrast, CS-1.2 (2), CS-2.1 (3), and SS (4) showed low or undetectable SERS responses with NIR wavelength excitation. More importantly, HS (1) is open to the environment, which is not the case for the closed-shell structures, giving chance molecules to access in the nanogap. The NIR-sensitive, wavelength-independent SERS responses of half-shell nanoparticles with sub-1.0-nm "open" nanogaps provide new opportunities to detect chemical species of interest at low concentrations, regardless of the excitation wavelength.

Experimental Section

DNA-mediated Au shell formation

For Au shell formation reactions, Cy3-modified thiolated ssDNA [3'-HS-Cy3-$(CH_2)_3$-A_{10}-PEG_9-AAACTCTTTGCGCAC-5'] was modified on Au NPs (20 nm, 1.0 nM) using the standard salt-aging method.[7, 25, 26] For a typical preparation of Au-NNPs, which were closed-shell structures with a narrow intra-nanogap (1.2 nm) in this study, a seed solution of DNA-AuNPs in deionized water (DW; 100 µL of a 1.0 nM solution) was mixed with 10 µL of 100 mM phosphate buffer (PB; pH 7.4) and 16.5 µL of 2.0 M NaCl to adjust to 0.3 M PBS condition and 50 µL of a 1.0% (w/v) poly(N-vinyl-2-pyrrolidone) solution (MW: 40,000, PVP). For a half-shell formation, the addition of the phosphate buffer and NaCl are not required. For a star-shaped nanoparticle formation, 10 µL of 100 mM PB (pH 8.0) was added to the seed solution without the addition of NaCl. To form an Au shell from each seed solution, 50 µL of a NH_2OH solution (10 mM) and 50 µL of a $HAuCl_4$ solution (5.0 mM) were subsequently added and the solution was shaken vigorously for 2 min. After standing solutions at room temperature for 2 h, it was centrifuged (5,000 rpm/15 min) to remove reactants and PVP in the supernatant and then redispersed in distilled water with 0.1% sodium dodecyl sulfate solution to prevent particle aggregation (See Supporting Information and Figure S1 for synthetic details).

Reaction kinetics study

For reaction parameter-dependent kinetics study, UV-vis spectrophotometer was used to measure the changes of the intensity of extinction at 520 nm during reactions.

Solution-based Raman analysis

For solution-based Raman analysis, three excitation wavelengths (532 nm, 660 nm and 785 nm) were used to study the SERS intensity of Cy3 molecules localized at intra-nanogap of resulting nanoparticle solution. The number of Cy3 molecules on the core DNA-AuNPs was same in all nanostructures in this paper. The concentration of nanoparticle solution was 0.5 nM, the exposure time to acquire Raman spectra was 1.0 sec and the laser power at sample was 1.0 mW.

Single particle-correlated Raman analysis

To clearly elucidate the plasmonic properties of anisotropic nanostructures with different Au shell and intra-nanogap distances,[27] we performed single particle-based correlated measurements between Rayleigh scattering and SERS responses using an atomic force microscopy (AFM)-correlated nano-Raman microscope equipped with a laser scanning-assisted dark-field configuration.[28] A confocal Rayleigh mapping with a small scan size (<1 µm) was performed prior to collecting the Rayleigh scattering spectrum with Xe-lamp excitation.[28] In such cases, an accurate Rayleigh scattering spectrum of the selected nanoparticle of interest can be obtained by precisely positioning the selected nanoparticle onto the optic axis of the objective.

Results and discussion

Figures 1a and 1b show high-resolution transmission electron microscope (HR-TEM) images and sketches, respectively, of the four different unique nanostructures: HS (1) generated from DW, CS-1.2 (2) from neutral buffer (pH 7.4 with NaCl), CS-2.1 (3) from basic buffer (pH 8.0 with NaCl), and SS (4) from basic buffer (pH 8.0 without NaCl). The intra-nanogap distances of HS (1) ranged from 0.5 to 1.2 nm, with a mean gap distance of 0.9 nm. CS-1.2 (2) showed a narrow distribution between 0.9 and 1.7 nm, with a mean gap distance of 1.2 nm. CS-2.1 (3) and SS (4) showed wide nanogap distributions ranging from 1.0 to 3.2 nm (mean gap distance: 2.1 nm) and from 1.5 to 4.2 nm (mean gap distance: 2.9 nm), respectively (Figure 1c). CS-1.2 (2) and CS-2.1 (3) show the characteristic LSPR spectra of spherical nanostructures at ~520 nm (red color, Figure 1d).

Journal of Materials Chemistry C Accepted Manuscript

This journal is © The Royal Society of Chemistry 20xx

Please do not adjust margins

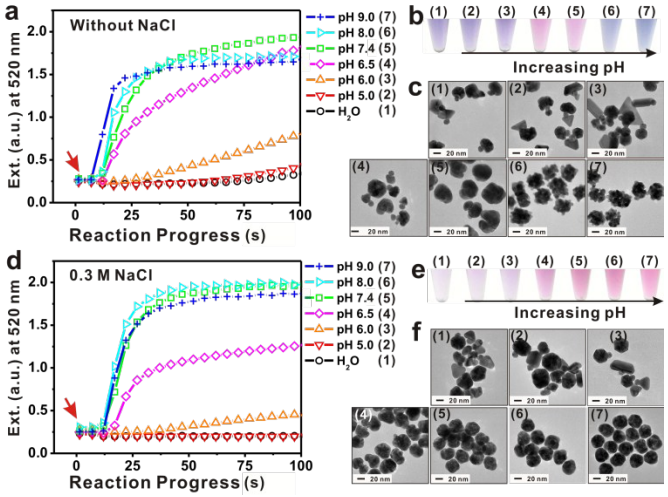

Figure 2. Reaction kinetics in various pH, salt content, and solution colors, and TEM images of the resulting nanostructures. (a) The reaction progress monitored by measuring optical density (OD) at 520 nm. (b) Solution color images. (c) Representative TEM images of particles prepared from distilled water and various pH conditions without NaCl (a–c) and with 0.3 M NaCl (d–f). (Red arrows in (a) and (d) indicate the addition of $HAuCl_4$).

However, much broader and red-shifted extinction spectra were observed for the HS (1) and SS (4) particles, whose solutions were blue, indicative of the anisotropic nature of these two nanostructures (Figures 1d and S2).

To understand the effects of the reaction conditions on the intra-nanogap distance and shell structures in detail, we monitored the reaction progress under various pH conditions (5.0, 6.0, 6.5, 7.4, 8.0, and 9.0) and in DW without NaCl (Figure 2a-2c) and with NaCl (Figure 2d-2e). The reaction progress was recorded every 5 s by measuring the optical density at 520 nm after the addition of the $HAuCl_4$ solution (red arrows in Figures 2a and 2d). The reaction in pure water without NaCl (Figure 2a, black circles) and with 0.3 M NaCl (Figure 2d, black circles) was very slow. The solution eventually turned a bluish color after 1.0 h at room temperature (Figures 2b-(1) and 2e-(1)). The HR-TEM images show the predominant formation of a half-shell structure (Figures 2c-(1) and 2f-(1)).

The reaction progress in weakly acidic solutions (pH 5.0 and 6.0) was also slow; the solutions at pH 5.0 (Figures 2c-(2) and 2f-(2)) exhibited almost the same reaction progress as the DW solution, whereas the solutions at pH 6.0 (Figures 2c-(3) and 2f-(3)) exhibited slightly faster reaction progress, which led to the formation of the half-shell structure and blue solution color. Although the particle solution prepared at pH 6.5 displayed a pale red color (Figure 2b-(4)), the particle shapes were not complete-shell structures but rather mixtures of complete-shell and half-shell structures (Figure 2c-(4)).

The reactions in weakly basic solutions (pH 8.0 and 9.0) were completed within 100 s after the addition of the precursor ($HAuCl_4$). The main structures under these conditions (pH 8.0 and pH 9.0) without NaCl were star-shaped Au shell nanostructures (Figures 2c-(6) and 2c-(7)) with a blue solution color (Figures 2b-(6) and 2b-(7)). In contrast, the reactions in pH 8.0 and 9.0 with 0.3 M NaCl resulted in the formation of spherical closed-shell structures (Figures 2f-(6) and 2f-(7)) with a bright red color (Figures 2e-(6) and 2e-(7)). The reaction at pH 7.4 without NaCl exhibited a non-uniform Au shell structure, as shown in Figure 2c-(5), whereas with 0.3 M NaCl, the formation of closed-shell structures was predominant with a strong red color (Figures 2e-(5) and 2f-(5)).

These results showed that low pH conditions (5.0, 6.0, 6.5) with DW resulted in slow reaction progress, which led to the predominant formation of anisotropic structures; however, neutral and basic pH conditions resulted in fast reaction progress, which led to the branched nanostructure formation. The presence of NaCl resulted in slow reaction progress, as summarized in Figure S3. To clarify the reaction rate depends on reaction conditions, the time-dependent solution color changes are also displayed in Figure S4, which is well agreement with the reaction progress in Figure 2d.

The effect of pH on the reaction kinetics and shell structures was further investigated using citrate-AuNPs or mPEG-modified AuNPs instead of DNA-AuNPs as the seed solution. The reactions in DW and at low pH resulted in slow reaction progress and relatively truncated Au shell structures with no intra-nanogap; however, the reaction in basic pH (8.0, 9.0) resulted in fast reaction progress and the predominant formation of highly branched (star-shaped) structures, as shown in Figures S5 and S6, which is the same phenomena that we observed with DNA-AuNPs at low and high pH.

These results indicate that the reaction kinetics and shell structures could be governed by the pH. The experimental results in this work were not consistent with that of known results for the pH-dependent ion species of $HAuCl_4$.[29, 30] It has been known that reactive chlorine-rich ion species ($[AuCl_{2.43}(OH)_{1.57}]$-, pH 5.01; $[AuCl_{1.09}(OH)_{2.91}]^-$, pH 6.16) are more dominant in acidic pH, whereas stable OH-rich ion species such as $[AuCl_{0.83}(OH)_{3.17}]^-$ and $[AuCl_{0.67}(OH)_{3.33}]^-$ are dominant at pH 7.52 and pH 8.01, respectively.[29, 31] But it should be noted that, in current work, the presence of excess PVP which is weak reducing agent and surfactant could significantly alter the reaction kinetics,[32, 33] especially when using a mild reducing agent (NH_2OH-HCl), which requires more detailed investigations.[30,34]

NaCl concentration was another key parameter for the formation of star-shaped structures because we have observed that only basic pH conditions without NaCl produced such nanostructures (Figures 2c-(6) and 2c-(7) and Figures 2f-(6) and 2f-(7)). The presence of NaCl could induce the formation of $AuCl_4^-$ ions, which would lead to slow reaction kinetics and the subsequent formation of uniform shell structures (Figures 2f-(6) and 2f-(7)). (Figure S3)

Table 1. Summary of reaction parameters and nanostructures.

	HS (1)	CS-1.2 (2)	CS-2.1 (3)	SS (4)
pH	5.0 or DW	7.4	8.0 or 9.0	8.0 or 9.0
NaCl	0 M	0.3 M	0.3 M	0 M
Time of completion*	3600 s	50 s	50 s	40 s
Nanogap distributions	0.5–1.3 nm	0.9–1.8 nm	1.0–3.2 nm	1.5–4.0 nm
Intra-nanogap distance (mean)	0.9 nm	1.2 nm	2.1 nm	2.9 nm

* Indicates the time required to reach the plateau of UV-vis absorption at 520 nm in the reaction progress (Fig. 2).

Above all, the most important factor for the formation of intra-nanogaps is the presence of oligonucleotides on the core AuNPs.[5] In acidic pH and pure water (pH 5.5), oligonucleotides prefer condensed structures.[35-37]

Journal of Materials Chemistry C Accepted Manuscript

Please do not adjust margins

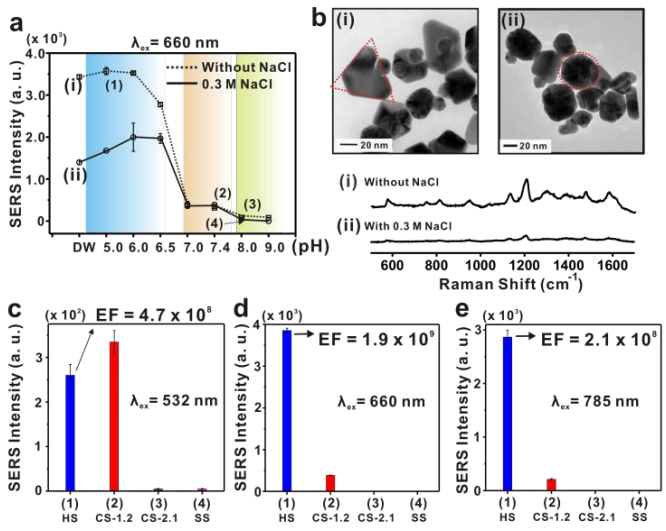

Figure 3. Raman responses of the nanostructures. (a) Raman intensity of all nanostructures prepared at various pH values without (dotted line) or with (black line) NaCl; the intensity of the Raman shift of Cy3 at 1200 cm^{-1} [λex = 660 nm, N = 5]) was selected for comparison. (b) Representative TEM images and Raman spectra of the particles prepared in (i) DW without NaCl or (ii) with 0.3 M NaCl. (c)–(e) Raman intensity of HS (1), CS-1.2 (2), CS-2.1 (3), and SS (4) analyzed at excitation wavelengths of (c) 532 nm, (d) 660 nm, and (e) 785 nm. (Particle concentration: 0.5 nM, exposure time: 1.0 s, power at sample: 1.0 mw).

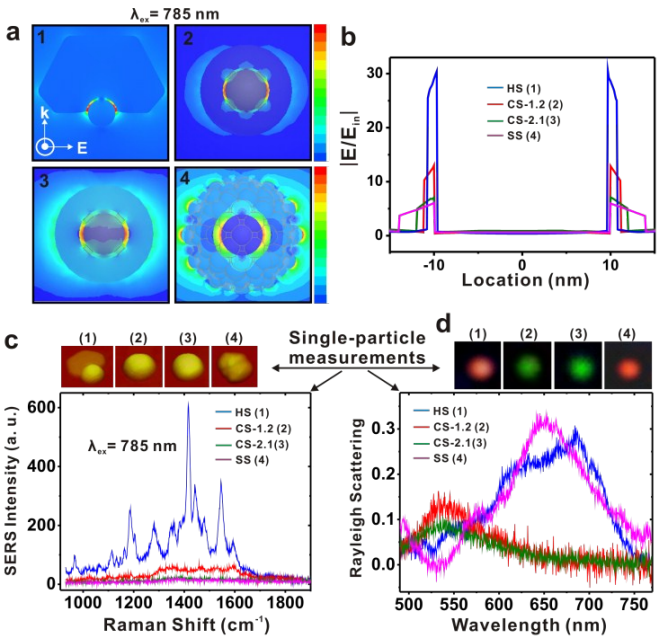

Figure 4. FEM-lab based simulations and AFM-correlated Raman measurement for single nanoparticles. (a) Finite element method (FEM)-based simulations and (b) line plot of electromagnetic field distributions along the center-horizontal line at an incident wavelength of 780 nm. (c) SERS spectra and AFM images (inset) of single half-shell [HS (1), blue], closed-shell with 1.2 nm intra-nanogap [CS-1.2 (2), red], closed-shell with 2.1 nm intra-nanogap [CS-2.1 (3), green], and star-shaped [SS (4), magenta] with irregular nanogap (785 nm). (d) Rayleigh scattering spectra and scattering images of HS (1), CS-1.2 (2), CS-2.1 (3), and SS (4).

The strong interactions between the adenine base and the gold surface are predominant in acidic pH conditions.[37] Both lead to the formation of an efficient protective layer of DNA on gold,[38] which can minimize the nucleation sites on the gold surface, subsequently inducing anisotropic shell growth to form a half-shell structure (Figure S7). In neutral and weakly basic pH (>7.0) conditions, the non-condensed conformation of oligonucleotides results in increased exposure of the gold surface, providing multiple nucleation sites for efficient catalytic reactions on the core gold surface, which can lead to relatively uniform Au shell structures with intra-nanogaps.[35, 39] The repulsion between negative ion species ($[AuCl_{0.67}(OH)_{3.33}]^-$) and the negative charge of the phosphate backbone in basic pH (>8.0) conditions can result in limited catalytic reduction on the gold surface owing to the repulsion of the negatively charged ion species of the precursor. The fast reaction kinetics in this basic pH (>8.0) ultimately results in the formation of a wider nanogap distance and an irregular shell structure.

Solution-based SERS measurements were performed to investigate the SERS response of the nanostructures with different shell structures and intra-nanogap distances. Figure 3a shows the SERS responses for all nanostructures prepared from DW, acidic (pH 5.0, 6.0), neutral (pH 6.5, 7.0, 7.4), and basic (pH 8.0, 9.0) conditions with and without NaCl. The incident wavelength was 660 nm and the SERS intensity at 1200 cm^{-1} was selected for comparison. HS (1) synthesized from DW, pH 5.0, and pH 6.0 conditions without NaCl (dotted line) exhibited much higher SERS intensities as compared to CS-1.2 (2) prepared in pH 7.4 with NaCl. However, no noticeable SERS intensity was measured for CS-2.1 (3) and SS (4) prepared from particle solutions at pH 8.0 without and with NaCl. The particle solutions prepared from DW and acidic pH (5.0, 6.0) with NaCl (open square solid line) exhibited considerably lower SERS intensity as compared to the particle solution prepared under the same conditions without NaCl (open circle dotted line). From the TEM images in Figure 3b, the particle solution in DW without NaCl shows more predominant formation of half-shell structures [red-dotted triangle in Figure 3b-(i)], whereas the particle solution prepared in DW with NaCl shows a higher fraction of spherical shell structures [shown as a red-dotted circle in Figure 3b-(ii)]. Thus, the strong SERS responses of half-shell nanoparticles prepared without NaCl is attributable to the high yield of half-shell structures (Figure 3b).

The nanoparticle solutions numbered (1)–(4) in Figure 3a correspond to HS (1), CS-1.2 (2), CS-2.1 (3), and SS (4), respectively. As shown in Figures 3c–e, HS (1) exhibited strong SERS responses to all three excitation wavelengths (532, 660, and 785 nm), whereas CS-1.2 (2) showed a strong SERS response only to the 532 nm excitation. No noticeable SERS response was observed from CS-2.1 (3) and SS (4) for any of the three excitation wavelengths, mainly due to the wide intra-nanogap distance of CS-2.1 (3) and the irregular intra-nanogap distance of SS (4). Considering the off-resonance effect of the Cy3 molecules at 660 and 785 nm wavelengths, such a prominent SERS response of HS (1) at the 660 nm and 785 nm wavelengths is expected to have originated from the highly enhanced electromagnetic field as a result of resonant excitation with the multiple LSPR modes and the narrow intra-nanogap (<1.0 nm).[40] Although SS (4) also has multiple LSPR modes resonant with NIR, the intra-nanogap distance of SS (4) was wider than 2.0 nm and irregular.

The SERS enhancement factors of HS (1) for the three different wavelengths were calculated to be 4.7×10^8 (532 nm), 1.9×10^9 (660 nm), and 2.1×10^8 (785 nm). When the EM field distributions around nanoparticles with a 785 nm incident wavelength were simulated, as shown in Figures 4a and 4b, the EF values in the nanogaps of HS (1), CS-1.2 (2), CS-2.1 (3),

Journal of Materials Chemistry C Accepted Manuscript

This journal is © The Royal Society of Chemistry 20xx

Please do not adjust margins

and HS (4) were calculated to be 1.5×10^6, 4.7×10^4, 0.2×10^4, 0.5×10^3, respectively.[7] The sub-1.0-nm nanogap and strong coupling of HS (1) with the 785 nm wavelength induced a highly enhanced and localized electromagnetic field, which resulted in 10 times stronger SERS responses as compared with CS-1.2 in the solution-state analysis.

To clearly elucidate the origin of excitation wavelength-dependent SERS responses,[27] we performed single particle-based correlated measurements between Rayleigh scattering and SERS responses using an atomic force microscopy (AFM)-correlated nano-Raman microscope equipped with a laser scanning-assisted dark-field configuration (Figures 4c and 4d).[28] The AFM images of the nanostructures are well matched with those of the HR-TEM analysis, as shown in the Figure 4c. Consistent with the solution-based SERS results with 785 nm excitation (Figure 3e), the single HS (1) nanoparticle showed the most pronounced SERS intensity among the structures (Figure 4c). The corresponding Rayleigh scattering spectra and dark-field image of HS (1) were also simultaneously obtained (Figure 4d, blue line). The background-subtracted Rayleigh scattering spectra showed multiple LSPR modes in HS (1), which is strongly related to the wavelength-independent SERS response observed in the solution-state analysis (Figures 3c–e).

The multiple LSPR modes indicate the presence of diverse plasmon coupling modes in the structures. When SERS signals from one hundred individual HS (1) nanoparticles were measured, the results showed narrow SERS intensity distribution on the order of 10^1. On the other hand, a single CS-1.2 (2) nanoparticle showed very weak SERS response in this analysis, with Rayleigh scattering spectra around 540 nm and a green scattering color (Figures 4c and 4d, red line and inset). A single CS-2.1 (3) particle showed very weak SERS response in this analysis, with Rayleigh scattering spectra around 650 nm and a red scattering color (Figures 4c and 4d, green line and inset). In spite of the broad Rayleigh scattering spectra of SS (4) at 650 nm (red scattering image in Figure 4d-inset), the single SS (4) particle showed an undetectable SERS response. These results confirm that multiple LSPR modes with sub-1.0-nm nanogaps are a critical factor for the wavelength-insensitive strong Raman response of HS (1).

Conclusions

In conclusion, we found that two key factors in DNA-mediated Au shell formation reactions, pH and NaCl, both strongly influence the DNA conformation and stability of precursor ion species, and thus they play a critical role in determining the optical properties of the resulting nanostructures by changing the shell structure and intra-nanogap distance. The new half-shell nanostructures with open sub-1.0-nm intra-nanogaps showed much stronger NIR-sensitive SERS responses as compared with previously reported closed intra-nanogap structures [CS-1.2 (2), Au-NNPs]. In addition, the wavelength-insensitive SERS responses with an open nanogap can open new opportunities for *in-situ* detection of chemical species in solution. Moreover, the sub-1-nm gap (Sub-One-Nanometer Gap; SONG) play a critical role in detecting molecules with high sensitivity based on the strong nanogap plasmon enhancement.[41, 42] From the correlated measurements at a single particle level, we accurately elucidated the optical properties of four different nanostructures. Understanding the detailed reaction conditions in controlling intra-nanogap distance and shell structures can provide new insights in designing plasmonic nanostructures suitable for plasmon-enhanced sensing applications.

Acknowledgements

This work was supported by the National Research Foundation (2013R1A1A1061387) and the KU-KIST research funds. Y.D.S. was supported by KRICT (SI-1509), the Industrial Strategic Technology Development Program (nos. 10033183 and 10037397) funded by the Ministry of Trade, Industry, and Energy (MI, Korea), and the Degree and Research Center (DRC) Program (2014) through the National Research Council of Science & Technology (NST) from the Ministry of Science, ICT and Future Planning. H.L. acknowledges financial support from the Public Welfare & Safety Research Program through NRF funded by MEST (2011-0020957).

Notes and references

1. S. J. Tan, M. J. Campolongo, D. Luo and W. Cheng, *Nat Nanotechnol.,* 2011, **6**, 268-276.
2. B. Ding, Z. Deng, H. Yan, S. Cabrini, R. N. Zuckermann and J. Bokor, *J. Am. Chem. Soc.*, 2010, **132**, 3248-3249.
3. W. Cheng, M. J. Campolongo, J. J. Cha, S. J. Tan, C. C. Umbach, D. A. Muller and D. Luo, *Nat. Mater.*, 2009, **8**, 519-525.
4. D. Nykypanchuk, M. M. Maye, D. van der Lelie and O. Gang, *Nature*, 2008, **451**, 549-552.
5. Z. Wang, J. Zhang, J. M. Ekman, P. J. A. Kenis and Y. Lu, *Nano Lett.*, 2010, **10**, 1886-1891.
6. Z. Wang, L. Tang, L. H. Tan, J. Li and Y. Lu, *Angew. Chem. Int. Edit,* 2012, **51**, 9078-9082.
7. D.-K. Lim, K.-S. Jeon, J.-H. Hwang, H. Kim, S. Kwon, Y. D. Suh and J.-M. Nam, *Nat Nanotechnol.,* 2011, **6**, 452-460.
8. J. W. Kang, P. T. C. So, R. R. Dasari and D.-K. Lim, *Nano Lett.*, 2015, **15**, 1766-1772.
9. J. Song, B. Duan, C. Wang, J. Zhou, L. Pu, Z. Fang, P. Wang, T. T. Lim and H. Duan, *J. Am. Chem. Soc.*, 2014, **136**, 6838-6841.
10. M. Li, T. Lohmüller and J. Feldmann, *Nano Lett.*, 2015, **15**, 770-775.
11. C. Ayala-Orozco, C. Urban, M. W. Knight, A. S. Urban, O. Neumann, S. W. Bishnoi, S. Mukherjee, A. M. Goodman, H. Charron, T. Mitchell, M. Shea, R. Roy, S. Nanda, R. Schiff, N. J. Halas and A. Joshi, *ACS Nano*, 2014, **8**, 6372-6381.
12. N. Gandra and S. Singamaneni, *Adv. Mater.*, 2013, **25**, 1022-1027.
13. J. Shen, L. Xu, C. Wang, H. Pei, R. Tai, S. Song, Q. Huang, C. Fan and G. Chen, *Angew. Chem. Int. Edit,* 2014, **53**, 8338-8342.
14. J.-W. Oh, D.-K. Lim, G.-H. Kim, Y. D. Suh and J.-M. Nam, *J. Am. Chem. Soc.*, 2014, **136**, 14052-14059.
15. J.-H. Lee, M.-H. You, G.-H. Kim and J.-M. Nam, *Nano Lett.*, 2014, **14**, 6217-6225.
16. E. Hao, S. Li, R. C. Bailey, S. Zou, G. C. Schatz and J. T. Hupp, *J. Phy. Chem. B*, 2004, **108**, 1224-1229.
17. J. B. Jackson and N. J. Halas, *Proc. Natl. Acad. Sci.*, 2004, **101**, 17930-17935.

Journal of Materials Chemistry C Accepted Manuscript

18. G. Liu, Y. Li, G. Duan, J. Wang, C. Liang and W. Cai, *ACS Appl. Mater. Inter.*, 2012, **4**, 1-5.
19. L. Rodríguez-Lorenzo, R. A. Álvarez-Puebla, F. J. G. de Abajo and L. M. Liz-Marzán, *J. Phy. Chem. C*, 2010, **114**, 7336-7340.
20. H. Yuan, Y. Liu, A. M. Fales, Y. L. Li, J. Liu and T. Vo-Dinh, *Anal. Chem.*, 2013, **85**, 208-212.
21. M. Li, J. W. Kang, R. R. Dasari and I. Barman, *Angew. Chem.*, 2014, **126**, 14339-14343.
22. S. T. Jones, R. W. Taylor, R. Esteban, E. K. Abo-Hamed, P. H. H. Bomans, N. A. J. M. Sommerdijk, J. Aizpurua, J. J. Baumberg and O. A. Scherman, *Small*, 2014, **10**, 4298-4303.
23. Z. Zhang, S. Zhang and M. Lin, *Chem. Commun.*, 2013, **49**, 8519-8521.
24. Y. Xia, Y. Xiong, B. Lim and S. E. Skrabalak, *Angew. Chem. Int. Edit*, 2009, **48**, 60-103.
25. S. J. Hurst, A. K. R. Lytton-Jean and C. A. Mirkin, *Anal. Chem.*, 2006, **78**, 8313-8318.
26. C. A. Mirkin, R. L. Letsinger, R. C. Mucic and J. J. Storhoff, *Nature*, 1996, **382**, 607-609.
27. E. M. Perassi, C. Hrelescu, A. Wisnet, M. Döblinger, C. Scheu, F. Jäckel, E. A. Coronado and J. Feldmann, *ACS Nano*, 2014, **8**, 4395-4402.
28. H. Lee, J.-H. Lee, S. M. Jin, Y. D. Suh and J.-M. Nam, *Nano Lett.*, 2013, **13**, 6113-6121.
29. S. Wang, K. Qian, X. Bi and W. Huang, *J. Phy. Chem. C*, 2009, **113**, 6505-6510.
30. C. Kan, W. Cai, C. Li and L. Zhang, *J. Mater. Res.*, 2005, **20**, 320-324.
31. X. Ji, X. Song, J. Li, Y. Bai, W. Yang and X. Peng, *J. Am. Chem. Soc.*, 2007, **129**, 13939-13948.
32. Y. Xiong, I. Washio, J. Chen, H. Cai, Z.-Y. Li and Y. Xia, *Langmuir*, 2006, **22**, 8563-8570.
33. M. Grzelczak, J. Pérez-Juste, P. Mulvaney and L. M. Liz-Marzán, *Chem. Soc. Rev.*, 2008, **37**, 1783-1791.
34. Lide, David R., ed. (2006). CRC Handbook of Chemistry and Physics (87th ed.). Boca Raton, FL: CRC Press. ISBN 0-8493-0487-3.
35. E. Cheng, Y. Xing, P. Chen, Y. Yang, Y. Sun, D. Zhou, L. Xu, Q. Fan and D. Liu, *Angew. Chem.*, 2009, **121**, 7796-7799.
36. C. Chen, G. Song, J. Ren and X. Qu, *Chem. Commun.*, 2008, 6149-6151.
37. F. Wang, B. Liu, P.-J. J. Huang and J. Liu, *Anal. Chem.*, 2013, **85**, 12144-12151.
38. M. R. Jones, K. D. Osberg, R. J. Macfarlane, M. R. Langille and C. A. Mirkin, *Chem. Rev.*, 2011, **111**, 3736-3827.
39. K. R. Brown and M. J. Natan, *Langmuir*, 1998, **14**, 726-728.
40. G. C. S. a. R. P. V. Duyne, *John Wiley & Sons*, 2006.
41. D. R. Ward, F. Hüser, F. Pauly, J. C. Cuevas and D. Natelson, *Nat Nanotechnol.,* 2010, **5**, 732-736.
42. H. Im, K. C. Bantz, N. C. Lindquist, C. L. Haynes and S.-H. Oh, *Nano Lett.*, 2010, **10**, 2231-2236.

Journal of Materials Chemistry C Accepted Manuscript

This journal is © The Royal Society of Chemistry 20xx

Please do not adjust margins

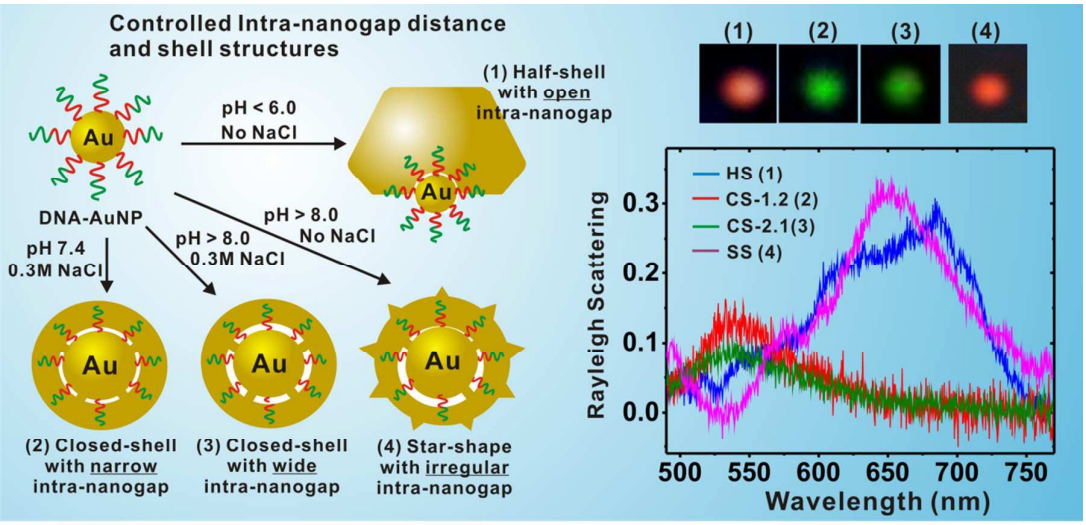

DNA-mediated simple synthetic methods enabled to obtain anisotropic plasmonic nanostructures with a tailorable intra-nanogap distance ranging from 0.9 to 4.0 nm.

Journal of Materials Chemistry C Accepted Manuscript